Investigation of transverse momentum distributions for fragments produced in reactions of ^{197}Au and ^{208}Pb projectiles with different targets in the energy range from 1.0 to 158 GeV/nucleon

G. Hüntrup, T. Streibel, and W. Heinrich
Department of Physics, University of Siegen, D-57068 Siegen, Germany
(Received 28 December 1999; revised manuscript received 30 July 2001; published 3 December 2001)

We have analyzed fragmentation processes of ^{197}Au and ^{208}Pb projectiles in reactions with targets ranging from CH_2 to Pb at projectile energies between 1.0 and 158 GeV/nucleon. For these experiments we used stacks consisting of foils of the plastic nuclear track detector material CR-39($C_{12}H_{18}O_7$). This detector material allows us to measure the charges and trajectories of relativistic particles with charges above a detection threshold Z_t. In this paper we analyze target and projectile energy dependences of transverse momentum distributions for projectile fragments produced in different fragmentation processes such as spallation, fission, and multifragmentation. Furthermore, for multifragmentation processes multiplicity dependences of the transverse momenta were studied. We found that besides the statistically distributed Fermi momenta of the nucleons, Coulomb repulsion may significantly contribute to the transverse momenta of the fragment nuclei. For heavy target nuclei, contributions caused by the repulsion of the incoming projectile nucleus and also by the outgoing fragment nucleus have been observed. For fission-type reactions and for multifragmentation reactions, in which more than one heavy fragment is produced in an interaction, the mutual repulsion between the fragments contributes to the measured transverse momenta.

DOI: 10.1103/PhysRevC.65.014605 PACS number(s): 25.75.−q, 25.70.Pq, 25.70.De, 25.85.−w

I. INTRODUCTION

A simple model developed by Goldhaber [1], which considers the statistically distributed Fermi momenta of the nucleons in the projectile, can, based on momentum conservation, quite well reproduce transverse momentum distributions of fragment nuclei measured in experiments with light projectiles [2,3]. Experiments performed with heavier projectiles, however, have shown that in these interactions the statistical contribution due to momentum conservation accounts only for part of the observed transverse momentum of the produced fragments [4–7]. Additional contributions may be due to Coulomb repulsion and ''bounce-off'' [8] between projectile and target nucleus.

In this paper we present measured transverse momentum distributions of projectile fragments produced in different fragmentation processes, such as spallation, fission, and multifragmentation reactions. We have performed experiments with ^{208}Pb projectiles at 1.0 and 158 GeV/nucleon and ^{197}Au projectiles at 10.6 GeV/nucleon using targets ranging from CH_2 to Pb. This set of data permits us to investigate target and projectile energy dependences of transverse momentum distributions in a wide range of projectile energies. These investigations may allow us to disentangle the contributions of different processes to the measured transverse momenta. For our experiments we used stacks of thin nuclear track detector sheets consisting of CR-39($C_{12}H_{18}O_7$) and BP-1 (composition is given in Ref. [9]). With these detectors we measure the charges and trajectories of all relativistic fragments with charges above the detection threshold Z_t of the detector material. For CR-39 the detection threshold is $Z_t = 6$ or $Z_t = 7$, depending on the batch of material and for BP-1 the detection threshold in our experiments is $Z_t = 74$.

The results are compared to the Goldhaber model [1]. Furthermore the contribution of the Coulomb repulsion between the projectile and target nucleus is estimated based on a simple model that should be a good approximation for peripheral reactions.

II. EXPERIMENTAL METHOD

We have used experimental setups (shown schematically in Fig. 1) containing stacks of foils of plastic nuclear track detectors CR-39 (0.6 mm thickness) and BP-1 (2 mm thickness). The heavy ions penetrating the detector foils generate latent tracks along their path, which can be developed by etching in NaOH solution. A few foils arranged upstream from a target in the projectile detector are used to measure charges and trajectories of incoming beam particles. Downstream from the target, the foils of the fragment detector are used to measure charges and trajectories of outgoing projectile fragments that have been produced inside the target.

Gaps between the detector foils allow the separation of projectile fragments that are produced in the same interaction. These gaps were adapted to the projectile energy. The lengths of the stacks were 0.1, 0.3, and 1.2 m for the experiments with energy beams of 1.0, 10.6, and 158 GeV/nucleon, respectively. Table I summarizes some details of the different

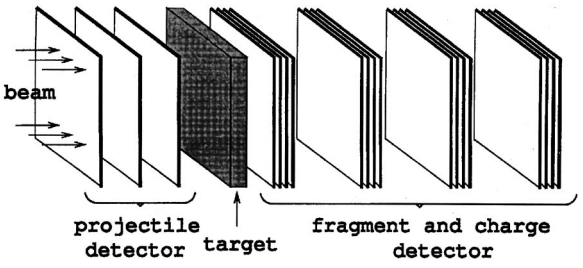

FIG. 1. Experimental setup for the experiments performed at 1.0, 10.6, and 158 GeV/nucleon.

TABLE I. Summary of the analyzed experiments.

Projectile	Energy (GeV/nucleon)	Target	Target thickness (cm)	Meas. fragments N_{tot}
^{208}Pb	1.0	CH_2	0.92 ± 0.02	18125
^{208}Pb	1.0	C	1.00 ± 0.02	21220
^{208}Pb	1.0	Cu	0.20 ± 0.01	8118
^{208}Pb	1.0	Pb	0.135 ± 0.01	4756
^{197}Au	10.6	CH_2	0.92 ± 0.02	73082
^{197}Au	10.6	C	1.45 ± 0.02	102491
^{197}Au	10.6	Pb	0.54 ± 0.02	32592
^{208}Pb	158	CH_2	0.92 ± 0.02	63349
^{208}Pb	158	C	1.45 ± 0.02	51309
^{208}Pb	158	Cu	0.40 ± 0.01	21061
^{208}Pb	158	Pb	0.54 ± 0.02	20282

experiments. N_{tot} indicates the total number of fragments observed.

The position and the size of all etch cones can be measured with an optical microscope system that is completely automated using the image analysis technique. For the reconstruction of the particle trajectories a precise alignment of the foils in the stack is necessary. This can be determined based on the track pattern of penetrating beam particles. After this alignment the position of an etch cone with respect to the fitted trajectory has a standard deviation of typically 1 to 2 μm. That means that, for example, for the 158 GeV/nucleon Pb experiment exposed at the CERN SPS in which a stack with a length of 1.2 m was used, the deflection of a fragment from the projectile direction can be measured with an accuracy of about 1 μm/1 m$=10^{-6}$. In the worst case, i.e., for a fragment with mass number $A=203$, this implies an uncertainty of the measured transverse momentum of 0.03 GeV/c. More details of the experimental setups are given in a separate paper [10].

For the determination of the transverse momenta the masses of the fragments are needed. However, the used experimental technique allows us only to measure the charges of the produced fragments. Furthermore, the velocity of the projectile fragments cannot be measured. Thus the fragment velocities and masses have to be estimated. We assume that the projectile fragments have (almost) the velocity of the incoming projectiles as has been observed in earlier experiments [2,11]. For the mass to charge assignment we use the EPAX code [12], which was determined in experiments with protons impinging on Au and Th targets at 2.6 GeV. Since this code does not consider the mass and charge numbers of the fragmenting nucleus, it may overestimate the mass change for projectile fragments with a charge number close to the charge number of the projectile, i.e., for fragments produced in extremely peripheral reactions. Therefore, for reactions with the ^{197}Au projectiles, we arbitrarily took the following charge and mass numbers: ($Z=78$, $A=192$ instead of $A=183$, which is the value predicted by EPAX); ($Z=77$, $A=187$ instead of $A=181$); ($Z=76$, $A=182$ instead of $A=178$); ($Z=75$, $A=177$ instead of $A=176$). For reactions with the ^{208}Pb projectiles we used: ($Z=81$, $A=203$ instead of $A=191$); ($Z=80$, $A=198$ instead of $A=189$); ($Z=79$, $A=193$ instead of $A=186$); ($Z=78$, $A=188$ instead of $A=183$). These mass numbers are integer values that are expected to be close to the mean mass value of all fragments produced with the charge number Z.

With these assumptions the transverse momenta p_F of the projectile fragments can be determined using the following relation:

$$p_F = A_F \sqrt{[(2m_n c^2) + E_p]E_p}\,\tan(\theta)/c, \qquad (1)$$

where A_F is the mass number of the projectile fragment, $m_n=931.5$ MeV is the mass of a bound nucleon, E_p is the kinetic energy per nucleon of the projectile, and θ is the deflection angle between the path of the incoming projectile and the outgoing fragment track.

For the low energy experiments at 1 GeV/nucleon it is possible to reconstruct for each individual fragmentation the interaction point inside the target in the coordinate direction along the stack axis with a precision better than 1 mm. That means that the energy of the projectile at the interaction point can be calculated based on the energy loss inside the penetrated detectors and target material. For the experiments at 10.6 GeV/nucleon and 158 GeV/nucleon the depths of the individual interaction points inside the target are known with much lower accuracy, however at this high energy the changes of E_p inside the target caused by the energy loss can be neglected. Thus uncertainties of E_p are not a significant source of errors for p_F. Main uncertainties arise from the estimation of A_F. One should keep in mind that our assumptions of specific fragment mass numbers may lead to systematic errors for the determined transverse momenta, which may be in the order of 203/191, i.e., about 6% for the extreme case of $\Delta Z=1$ reactions of the ^{208}Pb projectile.

III. TRANSVERSE MOMENTUM DISTRIBUTIONS

It has been observed already in the first experiments studying nuclear fragmentation with accelerated ions that the distribution of the transverse momentum components for fragments produced in reactions of light projectiles at rela-

tivistic projectile energies can be described by Gaussian functions [2,3].

These Gaussians are in good agreement with predictions of the statistical model of Goldhaber [1]. This model assumes that the Fermi momenta of the nucleons in a fragment are statistically distributed as those in the original projectile nucleus. Based on this assumption the Goldhaber model predicts that the variances $\sigma_G^2(A_F)$ for the distributions of the transverse momentum components for fragments with mass A_F are given by

$$\sigma_G^2(A_F)=\sigma_0^2\frac{A_F(A_P-A_F)}{(A_P-1)}, \tag{2}$$

where A_P is the mass number of the projectile, and $\sigma_0^2 = p_{Fermi}/5$. p_{Fermi} is the Fermi momentum of the nucleons.

For experiments with heavy projectile nuclei [4–7] also Gaussian functions were observed, but for fragments produced in collisions with target nuclei heavier than hydrogen, the experimentally determined variances $\sigma^2(A_F)$ are enlarged in comparison to the values $\sigma_G^2(A_F)$ predicted by the Goldhaber model [1]. This indicates that the Coulomb repulsion by the heavy target nucleus may contribute significantly. Furthermore a deviation from Gaussian functions has been observed in Ref. [7] for fragments produced in fission reactions of heavy projectile nuclei. We have investigated this subject in more detail with respect to the dependence on different types of fragmentation reactions, such as spallation, multifragmentation, and fission.

In our experiments we detect all fragments with Z_F above the threshold Z_t, which are emitted in an interaction. Fragmentation processes with only one large detected fragment can be interpreted as spallation reactions. In the case of only one small detected fragment probably a multifragmentation reaction has happened, in which due to the detection threshold of the detector material, only one single fragment was measured. Fragmentation processes with two detected fragments produced in the same interaction can be interpreted either as fission or as multifragmentation reactions with only two detected fragments. For the separation between these two processes we use the relation defined by [13]

$$Z_1Z_2 \geqslant \frac{Z_P^2}{9} \tag{3}$$

for candidates of fission events. Z_1 and Z_2 are the charges of the largest and the second largest fragment, and Z_P is the charge of the projectile. Furthermore we have analyzed events with three detected fragments produced in the same interaction. These events can be attributed to multifragmentation reactions.

A. Shape of the transverse momentum distributions

In Fig. 2 some typical transverse momentum component distributions are presented that were measured for fragments of 10 GeV/nucleon Au projectiles produced in collisions with C target nuclei. The experimental distributions are given by the histograms. Figure 2(a) shows the distribution for interactions where only one heavy fragment with a charge number $Z_F=77$ (i.e., mean mass number $A=187$) was observed ($M=1$), i.e., for fragments that are produced in spallation interactions. In Fig. 2(b) the distribution is shown for fragments with $Z_F=7$ (i.e., $A=14$) produced in interactions where two fragments were observed ($M=2$). By this criterion light fragments produced in multifragmentation reactions are selected. The same condition holds for the distribution shown in Fig. 2(c), where events with $Z_F=7$ ($A=14$) and $M=3$ were considered. Figure 2(d) shows the distribution for fragments that were produced in fission processes of the Au projectile. In these interactions two heavy fragments with charges $30 \leqslant Z_F \leqslant 38$ (i.e., mean mass $A=73$) were observed.

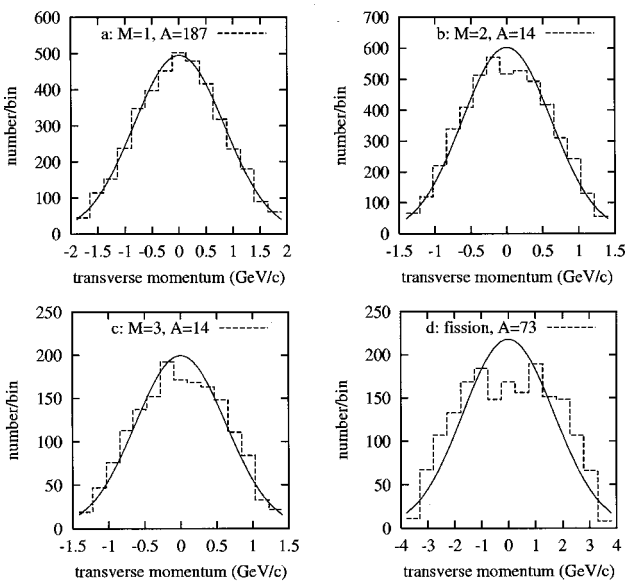

FIG. 2. Some examples for measured distributions of transverse momentum components for 10 GeV/nucleon Au projectiles in collision with C target nuclei: (a) for heavy fragments produced in spallation reactions, (b) and (c) for light fragments produced in multifragmentation reactions, and (d) for fragments produced in fission reactions.

For all measured distributions we determined the variances $\sigma_M^2(A_F)$. The curves drawn by lines in Fig. 2 are Gaussian functions with the experimentally determined variance. They have been normalized with respect to the total number of events. It is evident from Fig. 2(d) that for fission events the transverse momentum component distribution deviates significantly from a Gaussian function, whereas the other three distributions can be represented more or less accurately by Gaussian curves. This can be numerically investigated based on χ^2 values determined by a comparison of the experimental data and the curves. We get values of $\chi^2 = 12$, 52, 30, and 186 for the curves and data shown in Figs. 2(a)–2(d). Our distributions have 14 degrees of freedom, thus we expect $\chi^2=23.7$ for a confidence level of 95%.

Our experimentally determined variances $\sigma_M^2(A_F)$ have to be corrected for the influences of multiple scattering of the particles in the target and detector materials and for experimental errors of the measured transverse momenta. These

TABLE II. Parameters of the transverse momentum component distributions for some projectile fragments produced by 158 GeV/nucleon ^{208}Pb projectiles in collisions with CH_2 target. (For details see text.)

Proj.	Targ.	Z_F	M	A_F	σ_M (GeV/c)	σ (GeV/c)	χ^2	σ_G (GeV/c)	σ/σ_G	N_{tot}
^{208}Pb	CH_2	6	1	12	0.483	0.483	15	0.392	1.233	1492
^{208}Pb	CH_2	7	1	14	0.530	0.530	11	0.421	1.258	1032
^{208}Pb	CH_2	10–8	1	19	0.587	0.586	18	0.484	1.210	1900
^{208}Pb	CH_2	20–15	1	37	0.770	0.768	16	0.643	1.195	1834
^{208}Pb	CH_2	40–35	1	83	0.903	0.897	17	0.823	1.089	2456
^{208}Pb	CH_2	60–58	1	134	0.850	0.832	9	0.805	1.033	2452
^{208}Pb	CH_2	77	1	182	0.583	0.529	13	0.556	0.977	1962
^{208}Pb	CH_2	78	1	188	0.593	0.543	8	0.496	1.067	2072
^{208}Pb	CH_2	79	1	193	0.533	0.470	23	0.435	1.080	2392
^{208}Pb	CH_2	80	1	198	0.520	0.451	9	0.360	1.253	2400
^{208}Pb	CH_2	6	2	12	0.547	0.546	119	0.392	1.394	4836
^{208}Pb	CH_2	7	2	14	0.597	0.596	85	0.421	1.416	3174
^{208}Pb	CH_2	10–8	2	19	0.690	0.690	189	0.484	1.424	5882
^{208}Pb	CH_2	20–15	2	37	0.980	0.979	61	0.643	1.523	4542
^{208}Pb	CH_2	6	3	12	0.553	0.553	73	0.392	1.411	3008
^{208}Pb	CH_2	7	3	14	0.603	0.603	79	0.421	1.432	1846
^{208}Pb	CH_2	10–8	3	37	0.683	0.682	96	0.643	1.060	3380
^{208}Pb	CH_2	40–30	f	77	1.843	1.841	250	0.812	2.268	1760
^{208}Pb	CH_2	50–41	f	102	1.810	1.805	131	0.840	2.148	1300

corrections can be estimated based on the distribution of scattering angles θ_S between incoming and outgoing projectiles for which no interaction, neither in the target nor in the detector material, was detected. For all experiments the errors of θ_S are smaller than 1% due to the large number of noninteracting beam particles. Furthermore we assume that this distribution of scattering angles is the same for all fragments due to the fact that $\theta_S \sim Z_T$ (Z_T is the charge of the target nucleus). So we can determine the variances $\sigma_S^2(A_P)$ and $\sigma_S^2(A_F)$ of the contributions for the projectiles and projectile fragments caused by multiple scattering. With these values the measured variances $\sigma_M^2(A_F)$ can be corrected

$$\sigma^2(A_F) = \sigma_M^2(A_F) - \sigma_S^2(A_F). \tag{4}$$

The results for a set of distributions including fragments produced in different types of interactions are given in Tables II–VI. Data sets with a high statistical significance were selected for this purpose, which can be used to investigate the shape of the transverse momentum component distributions. Results for our 1 GeV/nucleon experiments, which have a lower statistical significance, were excluded. For the experiments performed for different projectile and target combinations at a higher energy, the values of the variance $\sigma_M^2(A_F)$ and the values $\sigma^2(A_F)$ corrected for multiple scattering and experimental errors are given in columns 6 and 7. As can be seen from the data presented in Tables II–VI the corrections for multiple scattering are small and negligible for small fragments, whereas they are significant for heavy fragments with small charge changes ΔZ between projectile and fragment. To get statistically significant results for the χ^2 values in some cases fragments with different charge number were grouped together. The value of χ^2 is given in column 8. Column 5 gives the mean mass number of the fragments. The last column gives the total number N_{tot} of measured tranverse momenta for the two components. For each interaction we measured the x and the y components. The different types of interactions are characterized by the multiplicity number M of observed fragments, which is given in column 4. Fission interactions are labeled by the letter f in this column. For a comparison with the Goldhaber model in column 9 calculated values of σ_G^2 are also given. For our experiments with ^{197}Au and ^{208}Pb projectiles we took a value of $p_{Fermi} = 265\,\text{MeV}/c$ as measured by Moniz *et al.* [14]. The ratio of σ/σ_G is given in column 10.

Figure 3 shows a scatterplot of the normalized variance σ/σ_G against χ^2 for the data of Tables II–VI. Different types of interactions are represented by different symbols. $M=1$ events, which for larger values of Z_F are spallation events are represented in Fig. 3 by circles. They typically have χ^2 values below about 25, i.e., their measured transverse momentum distributions can be well described by Gaussian functions. However, the variances of these distributions in some cases significantly exceed the values predicted by the Goldhaber model. As can be seen from the data presented in Tables II–VI this situation is typical for heavy spallation fragments produced in interactions with heavy target nuclei (Pb). Details of a comparison of the standard deviations of transverse momentum distributions with the predictions of the Goldhaber model will be discussed in the following section.

For fragments produced in fission reactions, which are shown by squares in Fig. 3, almost constant values of σ/σ_G between 2 and 2.5 are observed. For these events, as ob-

TABLE III. Parameters of the transverse momentum component distributions for some projectile fragments produced by 158 GeV/nucleon ^{208}Pb projectiles in collisions with C target. (For details see text.)

Proj.	Targ.	Z_F	M	A_F	σ_M (GeV/c)	σ (GeV/c)	χ^2	σ_G (GeV/c)	σ/σ_G	N_{tot}
^{208}Pb	C	6	1	12	0.490	0.489	13	0.392	1.249	2252
^{208}Pb	C	7	1	14	0.520	0.519	15	0.421	1.233	1460
^{208}Pb	C	10–8	1	19	0.587	0.586	16	0.484	1.209	2760
^{208}Pb	C	20–15	1	37	0.770	0.767	15	0.643	1.193	2334
^{208}Pb	C	40–35	1	83	0.927	0.913	15	0.823	1.109	2028
^{208}Pb	C	60–58	1	134	0.843	0.803	27	0.805	0.998	1690
^{208}Pb	C	77	1	181	0.653	0.553	15	0.565	0.979	1190
^{208}Pb	C	78	1	188	0.581	0.460	17	0.496	0.967	1256
^{208}Pb	C	79	1	193	0.577	0.442	17	0.435	1.016	1530
^{208}Pb	C	80	1	198	0.597	0.460	7	0.360	1.279	1460
^{208}Pb	C	6	2	12	0.543	0.543	72	0.392	1.385	4784
^{208}Pb	C	7	2	14	0.597	0.596	76	0.421	1.415	3390
^{208}Pb	C	10–8	2	19	0.670	0.669	86	0.484	1.381	5294
^{208}Pb	C	20–15	2	41	0.930	0.927	53	0.669	1.386	3926
^{208}Pb	C	6	3	12	0.540	0.540	57	0.392	1.377	2622
^{208}Pb	C	7	3	14	0.587	0.586	42	0.421	1.391	1642
^{208}Pb	C	10–8	3	19	0.683	0.682	76	0.484	1.409	2710
^{208}Pb	C	50–30	f	89	1.803	1.795	200	0.832	2.158	1692

served already above for the example in Fig. 2(d), the transverse momentum component distributions significantly deviate from Gaussian functions. As a result large χ^2 values are found. For fission reactions, where two large fragments are produced, it is expected that the transverse momenta of these fragments are dominated by the mutual Coulomb repulsion. These fragments should, therefore, move into directions distributed isotropically and have constant values of transverse momenta in the center-of-mass system. That means that their distribution of the total momentum is in this idealized picture a δ function. As a result the distributions of the transverse momentum components should be uniform distributions having a width that is defined by the total momentum of the fragments. However, it has to be considered that the total momentum, which a fission fragment gets by repulsion, depends on the charges of the two fission particles and on the original geometry, i.e., the distance of the emitted fission products. Experimentally a superposition of uniform distri-

TABLE IV. Parameters of the transverse momentum component distributions for some projectile fragments produced by 158 GeV/nucleon ^{208}Pb projectiles in collisions with Pb target. (For details see text.)

Proj.	Targ.	Z_F	M	A_F	σ_M (GeV/c)	σ (GeV/c)	χ^2	σ_G (GeV/c)	σ/σ_G	N_{tot}
^{208}Pb	Pb	6	1	12	0.460	0.455	27	0.392	1.162	1008
^{208}Pb	Pb	8–7	1	15	0.543	0.537	13	0.435	1.236	1102
^{208}Pb	Pb	12–9	1	22	0.637	0.626	17	0.517	1.210	1144
^{208}Pb	Pb	22–15	1	40	0.837	0.809	13	0.663	1.221	1076
^{208}Pb	Pb	64–58	1	140	1.410	1.193	24	0.789	1.513	1214
^{208}Pb	Pb	77–76	1	179	1.333	0.924	13	0.582	1.587	1568
^{208}Pb	Pb	78	1	188	1.243	0.725	25	0.496	1.510	1290
^{208}Pb	Pb	79	1	193	1.273	0.740	13	0.435	1.688	1686
^{208}Pb	Pb	80	1	198	1.278	0.710	20	0.360	1.756	1836
^{208}Pb	Pb	6	2	12	0.553	0.550	28	0.392	1.402	1592
^{208}Pb	Pb	7	2	14	0.617	0.612	38	0.421	1.453	1006
^{208}Pb	Pb	10–8	2	19	0.670	0.662	20	0.484	1.367	1732
^{208}Pb	Pb	20–15	2	37	0.993	0.973	29	0.643	1.514	1198
^{208}Pb	Pb	7–6	3	13	0.583	0.579	47	0.407	1.423	1298
^{208}Pb	Pb	12–8	3	21	0.747	0.738	28	0.506	1.457	1172
^{208}Pb	Pb	50–30	f	91	1.940	1.877	223	0.834	2.251	2294

TABLE V. Parameters of the transverse momentum component distributions for some projectile fragments produced by 10.6 GeV/nucleon ^{197}Au projectiles in collisions with C target. (For details see text.)

Proj.	Targ.	Z_F	M	A_F	σ_M (GeV/c)	σ (GeV/c)	χ^2	σ_G (GeV/c)	σ/σ_G	N_{tot}
^{197}Au	C	7	1	14	0.563	0.563	15	0.420	1.340	3382
^{197}Au	C	8	1	16	0.593	0.593	25	0.447	1.327	3466
^{197}Au	C	10–9	1	20	0.650	0.650	16	0.494	1.315	4894
^{197}Au	C	20–15	1	37	0.817	0.816	14	0.639	1.277	6830
^{197}Au	C	40–35	1	83	0.987	0.984	18	0.808	1.217	4362
^{197}Au	C	60–58	1	134	0.843	0.834	14	0.763	1.093	3080
^{197}Au	C	76	1	182	0.507	0.477	9	0.434	1.099	3100
^{197}Au	C	77	1	187	0.460	0.425	12	0.359	1.184	4128
^{197}Au	C	78	1	192	0.370	0.323	22	0.257	1.255	4568
^{197}Au	C	7	2	14	0.623	0.623	52	0.420	1.482	5022
^{197}Au	C	8	2	16	0.670	0.670	86	0.447	1.499	4752
^{197}Au	C	10–9	2	20	0.740	0.740	146	0.494	1.497	6952
^{197}Au	C	20–15	2	37	0.980	0.979	106	0.639	1.533	7694
^{197}Au	C	50–40	2	100	1.113	1.109	8	0.818	1.356	1864
^{197}Au	C	7	3	14	0.627	0.627	30	0.420	1.490	1662
^{197}Au	C	8	3	16	0.663	0.663	49	0.447	1.484	1470
^{197}Au	C	10–9	3	20	0.740	0.740	62	0.494	1.497	2056
^{197}Au	C	38–30	f	73	1.680	1.679	186	0.790	2.124	1814
^{197}Au	C	50–39	f	99	1.707	1.704	124	0.818	2.083	1326

butions of different widths should be observed. Additionally the observed distributions should be affected by the Coulomb repulsion of the incoming projectile from the target nucleus before the interaction and by the repulsion of the fission products from the target nucleus. The distribution shown in Fig. 2(d) is in agreement with the ideas discussed above.

The fact that mutual repulsion of the two fission fragments dominates their transverse momenta implies that for these fragments the variances of the transverse momentum components should be almost independent on the target type and on the projectile energy. This is observed in the experiments. For fission processes of ^{208}Pb projectiles in CH_2 and C targets for fragments with $79 \leqslant A_F \leqslant 98$ ($36 \leqslant Z \leqslant 44$) at 1.0 GeV/nucleon a mean value of $\sigma^2(A_F) = 1.83 \pm 0.03$ GeV/c was observed. At 158 GeV/nucleon one gets for the same projectile and target combinations in the same mass and

TABLE VI. Parameters of the transverse momentum component distributions for some projectile fragments produced by 10.6 GeV/nucleon ^{197}Au projectiles in collisions with Pb target. (For details see text.)

Proj.	Targ.	Z_F	M	A_F	σ_M (GeV/c)	σ (GeV/c)	χ^2	σ_G (GeV/c)	σ/σ_G	N_{tot}
^{197}Au	Pb	7	1	14	0.577	0.572	11	0.420	1.360	1742
^{197}Au	Pb	8	1	16	0.637	0.631	20	0.447	1.411	1348
^{197}Au	Pb	10–9	1	20	0.683	0.675	24	0.494	1.365	1686
^{197}Au	Pb	20–15	1	37	0.947	0.925	16	0.639	1.448	1954
^{197}Au	Pb	40–35	1	82	1.320	1.243	15	0.807	1.541	1108
^{197}Au	Pb	76–75	1	177	1.503	1.156	9	0.494	2.339	1462
^{197}Au	Pb	77	1	187	1.470	1.063	15	0.359	2.960	1168
^{197}Au	Pb	78	1	192	1.337	0.837	12	0.257	3.251	3190
^{197}Au	Pb	62–58	1	137	1.530	1.337	13	0.753	1.776	1298
^{197}Au	Pb	78–73	1	177	1.523	1.182	14	0.494	2.392	6672
^{197}Au	Pb	7	2	14	0.660	0.656	38	0.420	1.560	2064
^{197}Au	Pb	8	2	16	0.707	0.701	32	0.447	1.569	1462
^{197}Au	Pb	10–9	2	20	0.773	0.766	39	0.494	1.549	1880
^{197}Au	Pb	20–15	2	37	1.057	1.037	29	0.639	1.623	2034
^{197}Au	Pb	8–7	3	14	0.693	0.689	25	0.420	1.639	1140
^{197}Au	Pb	12–9	3	22	0.817	0.808	25	0.515	1.568	1172
^{197}Au	Pb	50–30	f	91	1.847	1.779	49	0.816	2.181	836

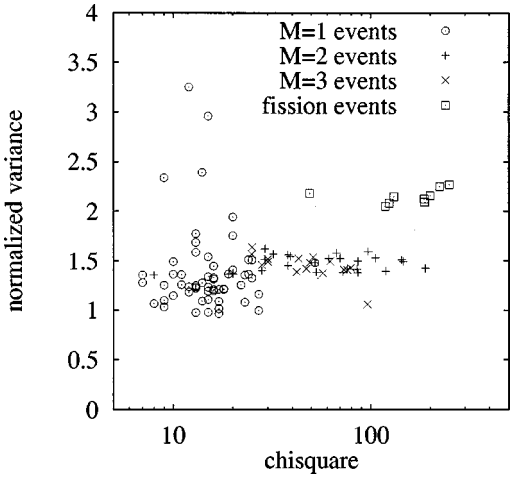

FIG. 3. Variance of the measured transverse momentum component distributions for the data presented in Table II is plotted against the χ^2 value of the distribution, which was determined by a comparison to a Gaussian distribution.

charge range a mean value of $\sigma^2(A_F)=1.77\pm0.03\,\mathrm{GeV}/c$. For the experiments with the ^{197}Au projectiles we found for reactions with the CH_2 and C target for fragments with $77\leqslant A_F\leqslant 94\,(34\leqslant Z\leqslant 42)$ a value of $\sigma^2(A_F)=1.70\pm0.03\,\mathrm{GeV}/c$.

For multifragmentation events (events with $M=2$ and $M=3$) that are represented by two different types of crosses in Fig. 3 the ratio σ/σ_G is about 1.5. For some reactions small χ^2 values can be found, which indicates that the momentum distributions can be represented by Gaussians, for other reactions the χ^2 value indicates significant deviations from Gaussian functions. As can be derived from the data presented in Tables II–VI large values of χ^2 are found especially for fragments with small masses produced in $M=2$ interactions with light targets CH_2 and C. Studies of correlations between the charges of fragments produced in the same interaction have shown [5,7,10] that $M=2$ events for the collision with light target nuclei contain a high contribution of so called associated spallation events, in which a light fragment is produced simultaneously with a heavy fragment. The transverse momenta of these two fragments, especially that one of the lighter partner, should also be significantly affected by the mutual Coulomb repulsion of the fragments and as a result the momentum component distributions should resemble to some extent the distributions of the fission fragments. On the other hand, in situations where mutual repulsion between the fragments should have a somewhat smaller effect also smaller values of χ^2 can be found in Tables II–VI, such as for the production of three light fragments ($M=3$ events) or for the $M=2$ events produced in collisions with heavy target nuclei, where associated spallation is a rare process.

B. Comparison of the variances of transverse momentum distributions to model predictions

In this section we will compare the measured variances of transverse momentum component distributions for spallation and multifragmentation interactions with predictions of the Goldhaber model. In Fig. 4 the results for $\sigma(A_F)$ for reactions of ^{208}Pb projectiles with the targets CH_2, C, Cu, and Pb at 1.0 GeV/nucleon are presented. Fission events defined by the condition of Eq. (4) were excluded. Due to somewhat different detection thresholds Z_t for the different experiments using the CR-39 detectors for this analysis only fragments with charge numbers $Z\geqslant 7$ are considered in this comparison for all experiments. Therefore, the results can be compared directly. The variances predicted by the statistical model of Goldhaber are shown as curves. For spallation reactions ($M=1$ and $A_F\geqslant 150$) of ^{208}Pb projectiles with the CH_2 target the data points agree quite well with the curves. However, for the other events with only one detected fragment ($M=1$ and $A_F<150$) the data points deviate significantly from the prediction. For the other heavier targets one finds, that also for the spallation reactions with $A_F\geqslant 150$ and $M=1$ the values of $\sigma(A_F)$ are enhanced in comparison to the model prediction. Furthermore an increase of this deviation with increasing target mass can be observed. This increase can be caused by the Coulomb repulsion between projectile and target nucleus and possibly by an additional contribution of ''bounce-off.'' For the multifragmentation reactions with two

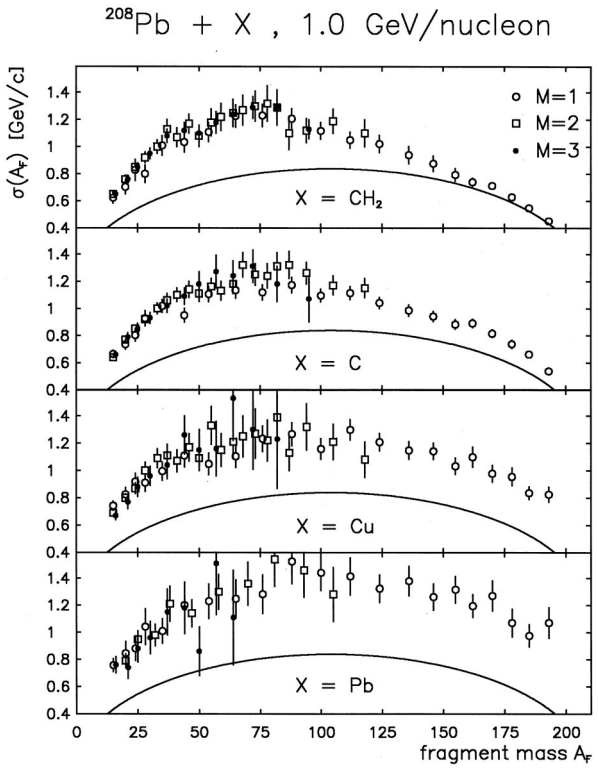

FIG. 4. Standard deviations $\sigma(A_F)$ are shown, which were determined from the measured distributions of the transverse momentum components for projectile fragments with mass A_F produced in reactions of ^{208}Pb projectiles with targets of CH_2, C, Cu, and Pb at a projectile energy of 1.0 GeV/nucleon. The results for interactions with only one detected fragment are shown by the open circles ($M=1$), results for events with two detected fragments (excluding fission events) are represented by the squares ($M=2$), and results for events with three detected fragments are shown as the filled circles ($M=3$).

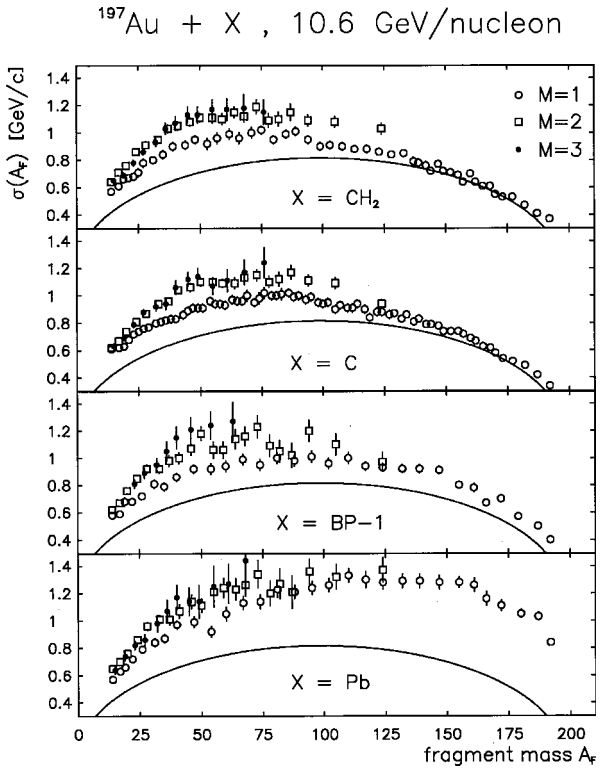

FIG. 5. $\sigma(A_F)$ as in Fig. 4 for projectile fragments produced in interactions of ^{197}Au projectiles with targets of CH_2, C, and Pb and the detector material BP-1 at a projectile energy of 10.6 GeV/nucleon. For the definition of the symbols see Fig. 4.

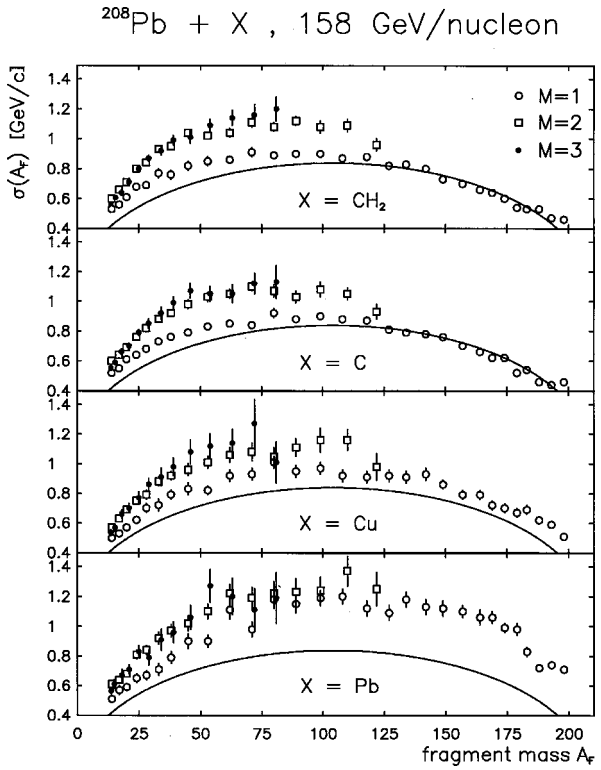

FIG. 6. $\sigma(A_F)$ as in Fig. 4 for projectile fragments produced in interactions of ^{208}Pb projectiles with targets of CH_2, C, Cu, and Pb at a projectile energy of 158 GeV/nucleon. For the definition of the symbols see Fig. 4.

($M=2$) or three ($M=3$) detected fragments the values of $\sigma(A_F)$ are considerably enhanced for all projectile target combinations compared to the predictions of the Goldhaber model. No statistically significant target size dependences can be observed for these interaction processes. Furthermore it should be stated that the results for events with one, two, or three detected fragments are identical within the error bars.

In Fig. 5 $\sigma(A_F)$ of the transverse momentum components for reactions of ^{197}Au projectiles with the targets CH_2, C, and Pb and the detector material BP-1 at 10.6 GeV/nucleon are presented. Again results for spallation and multifragmentation events with one, two, and three detected fragments are shown separately in this figure. One can observe that the general dependence on A_F is quite similar to that found for the experiments at 1.0 GeV/nucleon. As for the experiments at 1.0 GeV/nucleon for ^{208}Pb projectiles a significant target size dependence can be observed for the spallation reactions. However, the values for the experiment with the C target are at 10.6 GeV/nucleon significantly closer to the predictions of the Goldhaber model than at 1 GeV/nucleon.

The values of $\sigma(A_F)$ for the multifragmentation reactions for the experiments at 10.6 GeV/nucleon are somewhat smaller than for the results at 1.0 GeV/nucleon. This is most significant for the events with only one detected fragment and values of $A_F<125$, which, as mentioned above, very likely are multifragmentation events with one or more fragments having a charge $Z_F<Z_t$. At 1.0 GeV/nucleon for reactions with the light targets CH_2 and C the maximum values of $\sigma(A_F)$ for $M=1$ events can be found around $A_F=75$ and have a value of about $\sigma(A_F=75)=1.2\,\mathrm{GeV}/c$. At 10.6 GeV/nucleon we find maximum values of about $\sigma(A_F=75)=1.0\,\mathrm{GeV}/c$ for reactions with the light targets. For the other multifragmentation reactions with two or three detected fragments a weaker projectile energy dependence is observed.

Additionally at 10.6 GeV/nucleon a weak but significant target size dependence can be found for the multifragmentation reactions. This is most significant for the events with fragments having mass numbers $A_F \geqslant 100$, which were observed for $M=2$ interactions. Furthermore, similar as for the experiments at 1.0 GeV/nucleon, the results for the events with two and three detected fragments produced in the same interaction are identical within the error bars.

The results for the experiments with ^{208}Pb projectiles at 158 GeV/nucleon and the targets CH_2, C, Cu, and Pb are presented in Fig. 6. Again $\sigma(A_F)$ is shown separately for spallation and multifragmentation reactions. The results are in general similar to those observed for the experiments at the smaller projectile energies. But it is found that the values for $\sigma(A_F)$ at 158 GeV/nucleon are in general smaller than at 1.0 and 10.6 GeV/nucleon.

Again a significant target size dependence can be found for the spallation events. Furthermore, a comparison with the results at 1.0 GeV/nucleon reveals significant projectile energy dependences for the targets C, Cu, and Pb. At 158 GeV/nucleon $\sigma(A_F)$ of the transverse momentum distributions for the spallation processes for reactions, with the C target can be described almost perfectly by the Goldhaber model. Also

the values for reactions with the heavier targets Cu and Pb are significantly smaller at 158 GeV/nucleon than at 1.0 GeV/nucleon. For example, at $A_F=150$ one gets $\sigma(A_F=150)=1.3\,\mathrm{GeV}/c$ for the experiment with the Pb target at 1.0 GeV/nucleon. But for the same projectile target combination one observes a value of $\sigma(A_F=150)=1.15\,\mathrm{GeV}/c$ for the experiment at 158 GeV/nucleon. This strong projectile energy dependence can also be observed for the other fragmentation events with only one detected fragment with masses $A_F\leqslant 150$ that may be interpreted as multifragmentation events. But for these fragmentation processes a projectile energy dependence can be observed for all projectile target combinations. For reactions of ^{208}Pb projectiles with CH_2 we find for events with $M=1$ at $A_F=75$ values of about $\sigma(A_F=75)=1.2\,\mathrm{GeV}/c$ at 1.0 GeV/nucleon. For the same projectile target combination one gets at 158 GeV/nucleon values of about $\sigma(A_F=75)=0.9\,\mathrm{GeV}/c$.

As for the other projectile energies also at 158 GeV/nucleon $\sigma(A_F)$ is within the error bars identical for the multifragmentation reactions with two or three detected fragments. Furthermore, a weak projectile energy dependence can be recognized for these multifragmentation reactions with two or three detected fragments. One observes that the $\sigma(A_F)$ at 158 GeV/nucleon are about 10% smaller than at 1.0 GeV/nucleon.

Altogether for all analyzed reaction processes target and projectile energy dependences of the variations are observed, especially for the reactions with only one detected fragment produced in the interaction. Furthermore, it should be noted that $\sigma(A_F)$ depends on the multiplicity M for almost all fragment masses A_F, at least for the experiments at 10.6 and 158 GeV/nucleon. The values for $\sigma(A_F)$ for $M=1$ reactions are in general smaller than those for $M=2$ and $M=3$ reactions. This may be a hint that $M=1$ reactions at 10.6 and 158 GeV/nucleon with one small fragment can only partly be interpreted as multifragmentation reactions. There may be contributions by deep spallation reactions.

IV. INFLUENCE OF COULOMB REPULSION FOR SPALLATION REACTIONS

As can be inferred from the observed target size dependences of the variances of the transverse momentum component distributions for the spallation reactions, the Coulomb force between the projectile and target nuclei contributes significantly. We have tried to estimate this contribution by a simplified model calculation. For this purpose the repulsion of the incoming projectile nucleus and the outgoing fragment by the target nucleus was considered in a relativistically invariant calculation. A projectile nucleus impinges with an impact parameter b from infinity onto a target nucleus that is at the beginning at rest. The Coulomb force between the nuclei is determined for short time steps and the change of the momenta of the nuclei is calculated with the assumption that the Coulomb force is constant during these steps. In this calculation we consider the charge change of the projectile and the target nuclei in the collision by an approximation. The nuclei are described in a simple model as spheres with a radius of $1.35\,A_P^{1/3}$ fm and a homogenous nucleon density. During the interaction phase of the nuclei the overlapping parts of the two spheres are assumed to be abraded. These parts can be interpreted as the fireball particles. For the estimation of a lower limit of the Coulomb contribution only the Coulomb force between the nonabraded parts of the nuclei is calculated, which can be interpreted as the projectile and target spectators. The Coulomb force of the fireball particles on the spectators is not considered in this calculation. However, for the peripheral reaction processes due to the small number of participating nucleons in the interaction this simple model may be a reasonable estimate of the magnitude of the effect of Coulomb repulsion by the target nucleus.

After the interaction of the nuclei the target and projectile spectators are propagated in the Coulomb field of the other spectator, neglecting again the contribution of the fireball particles. Then the deflection angle between the incoming projectile and outgoing projectile spectator is determined. With this angle the transverse momenta caused by the Coulomb repulsion can be calculated using formula (1). By this calculation each impact parameter is associated with exactly one scattering angle, i.e., the momentum transfer.

The transverse momentum caused by Coulomb repulsion and also the size of the abraded projectile, which forms the prefragment, depends on the impact parameter of the collision. The prefragment is highly excited and emits nucleons or decays. Finally it ends in the ground state of one or several stable fragments with lower charge and mass number. As a result a stable fragment may originate from interactions within an interval of impact parameters. As a consequence, an interval of angles due to the Coulomb repulsion has to be expected. We avoid the problem of unknown distribution of impact parameters for an observed fragment by the restriction of our calculations to peripheral interactions where the mass difference between the excited prefragment and the stable fragment is small. We identify the mass of the prefragment with that one of the stable fragment and thus can correlate constant impact parameters with the fragment masses. By this procedure we, in principle, slightly overestimate in the calculation the masses and charges of the fragments produced in peripheral interactions.

In Fig. 7 we compare results for the reduced value $\sigma_{\mathrm{red}}(A_F)$ of the distributions for the transverse momentum components with the results of the estimations for the Coulomb contribution. $\sigma_{\mathrm{red}}(A_F)$ is defined as

$$\sigma_{\mathrm{red}}(A_F)=\sqrt{\sigma^2(A_F)-\sigma_G^2(A_F)}, \tag{5}$$

with $\sigma_G^2(A_F)$ giving the expected value based on the Goldhaber model as defined above in Eq. (2). In this figure the results for $\sigma_{\mathrm{red}}(A_F)$ for reactions of ^{208}Pb projectiles at 1.0 and 158 GeV/nucleon and of ^{197}Au projectiles at 10.6 GeV/nucleon with a Pb target are presented. The results for the estimation of the Coulomb contribution are shown by the dotted curves.

Considering the comparatively large statistical errors, one can state that at 1.0 GeV/nucleon the experimental results for fragment mass numbers $A_F\geqslant 150$ [10] are in agreement with the model predictions. For values of $A_F<150$ our simple model, which does not include effects caused by the fireball

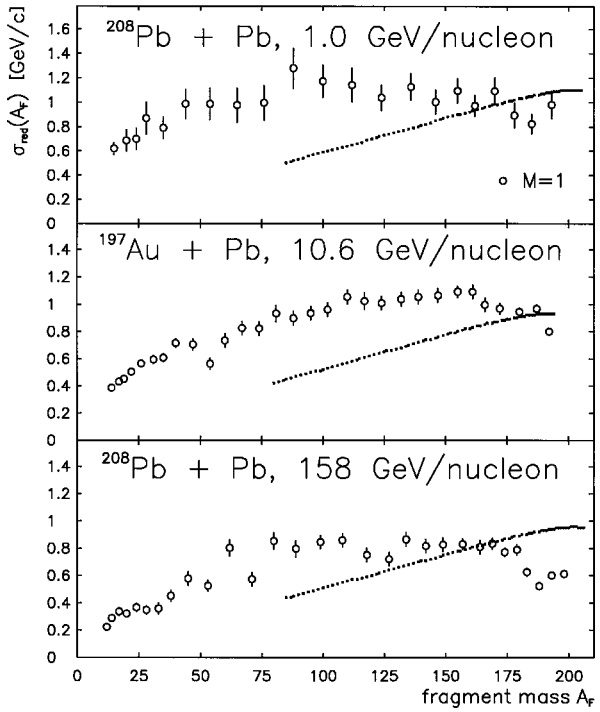

FIG. 7. Reduced standard deviation $\sigma_{\mathrm{red}}(A_F)$, i.e., the part of $\sigma(A_F)$ exceeding the predictions of the Goldhaber model, for the distribution of the transverse momentum components measured for reactions of ^{208}Pb projectiles at 1.0 and 158 GeV/nucleon and of ^{197}Au projectiles at 10.6 GeV/nucleon with a Pb target for events with $M=1$. The model calculations for the Coulomb contribution to the transverse momenta are represented by the dotted curves.

nucleons and does not consider a distribution of impact parameters, evidently fails. However, as discussed above we expect that our model is valid only for spallation reactions with small values of ΔA and ΔZ. For larger values of ΔA and ΔZ our model gives only a lower limit of the contribution of Coulomb repulsion to the transverse momenta of spallation fragments.

For the other experiments at 10.6 and 158 GeV/nucleon the statistical errors are rather small. Systematic uncertainties for $\sigma(A_F)$ are caused by the uncertainties of p_F as discussed above in connection with Eq. (1). These uncertainties are expected to be at maximum in the order of 5% for interactions with a charge change of $\Delta Z=1$. One observes, however, that at 10.6 GeV/nucleon one data point and at 158 GeV/nucleon at least four data points are significantly below the model predictions for large fragment masses A_F. If the reaction scenario used in our model calculation is correct, the experimental result for $\sigma_{\mathrm{red}}(A_F)$ should be equal or larger than the results for the model calculations. The small values of $\sigma_{\mathrm{red}}(A_F)$ can be understood as a hint for a different breakup process for the spallation reactions at the large projectile energies especially at 158 GeV/nucleon. We have reported a steep increase of the yields of fragments with charge for reactions of ^{208}Pb projectiles with a Pb target at 158 GeV/nucleon for $Z_F \geqslant 70$ (see Fig. 3 of [10]). This steep increase of the yield of spallation fragments with small values of ΔZ is caused by the electromagnetic dissociation process. In this reaction process the projectile nucleus is excited by the electromagnetic field of the target nucleus, which leads to the emission of nucleons. These reactions occur at impact parameters, which are larger than the sum of the radii of the two reacting nuclei. This different reaction process accounts for the observed small transverse momenta especially at 158 GeV/nucleon.

The reduced value $\sigma_{\mathrm{red}}(A_F)$ for reaction processes leading, for example, to a charge change of two charge units for ^{208}Pb projectiles at 158 GeV/nucleon can be reproduced by our model if we choose a mean impact parameter of about $b=22$ fm. This value of the impact parameter is significantly larger than the sum of the radii of two lead ions $r_T+r_P \approx 16$ fm. The comparison of the values for $\sigma_{\mathrm{red}}(A_F)$ with the model predictions shows that for reactions of ^{208}Pb projectiles with a Pb target at 158 GeV/nucleon fragments with charge changes by at least up to five units in comparison to the projectile are significantly influenced by the electromagnetic dissociation process. For reactions of ^{197}Au projectiles with a Pb target at 10.6 GeV/nucleon one finds, however, that only interactions with a charge change of one unit are significantly influenced by the electromagnetic dissociation process. These measurements confirm the conclusion of a large projectile energy dependence for the contribution of the electromagnetic dissociation process that was already inferred by the examination of the charge yields [10].

As discussed above for the spallation reactions with light targets the measured values of $\sigma(A_F)$ agree quite well with the predictions of the Goldhaber model. This can be seen in Figs. 4, 5, and 6 for the CH_2 target at all energies and for the C target for energies above 1 GeV/nucleon. For target nuclei with small charge numbers the Coulomb contributions are negligible, so that $\sigma_{\mathrm{red}}(A_F)$ is almost identical to $\sigma(A_F)$. The agreement of $\sigma(A_F)$ to the predictions of the Goldhaber model allows us to conclude that for these reactions the contribution of the electromagnetic dissociation is also rather small. However, this is expected due to the dependence of electromagnetic dissociation on the square of the charge number of the target nucleus.

V. TRANSVERSE MOMENTUM SUMS

In Figs. 4, 5, and 6 one can observe that the standard deviations $\sigma(A_F)$ of the distribution for the transverse momentum components for fragments with $M \geqslant 2$ (more than two fragments with $Z \geqslant 7$ produced in the same interaction) are for all projectile target combinations at all projectile energies considerably enhanced in comparison to the predictions of the statistical model of Goldhaber. Since this observation holds also for reactions with light targets, such as CH_2 and C, this deviation cannot be attributed to a Coulomb repulsion between target and projectile nucleus. Furthermore, one finds that the values for $\sigma(A_F)$ for fragments with $M \geqslant 2$ are at least at 10.6 and 158 GeV/nucleon significantly larger than for fragments with $M=1$. This may be caused by mutual Coulomb repulsion between the fragments produced in multifragmentation reactions.

To investigate this in more detail we determined the vector sum of the transverse momenta of the two fragments with

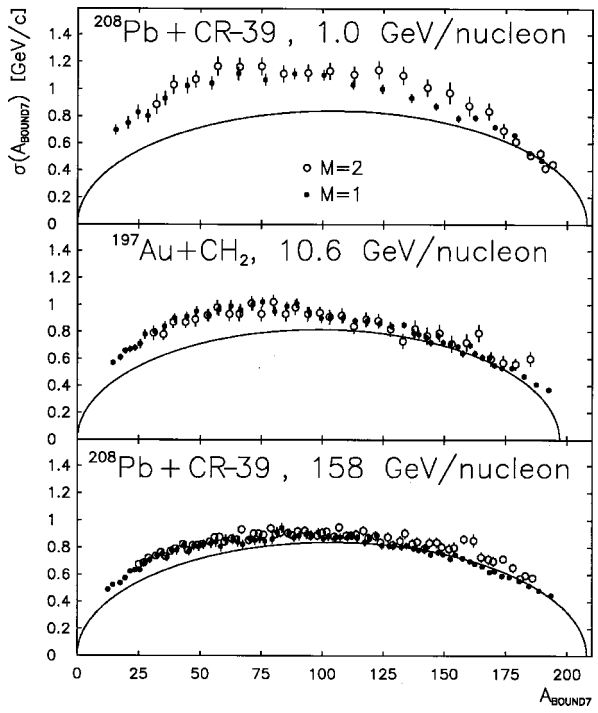

FIG. 8. Widths $\sigma(A_{BOUND7})$ for the distribution for the transverse momentum components measured for reactions of ^{208}Pb projectiles with the detector material CR-39 at 1.0 and 158 GeV/nucleon and for reactions of ^{197}Au projectiles with CH_2 at 10.6 GeV/nucleon as a function of the bound mass A_{BOUND7} for events with $M=2$ (open circles). These results are compared to the values determined for events with $M=1$ (filled circles).

$Z \geqslant 7$ produced in the same interaction for events with $M=2$. The mass of all fragments with $Z \geqslant 7$ produced in the same interaction is called A_{BOUND7}. In Fig. 8 we compare the results for the widths $\sigma(A_{BOUND7})$ for the distribution of the components for the transverse momentum sum with the results for $\sigma(A_F)$ for fragments with $M=1$ plotted as a function of the sum of the fragment masses A_{BOUND7}. We analyzed the results for reactions of ^{208}Pb projectiles with the detector material CR-39 at 1.0 GeV/nucleon, of ^{197}Au projectiles with CH_2 at 10.6 GeV/nucleon, and of ^{208}Pb projectiles with CR-39 at 158 GeV/nucleon. We have chosen results for these projectile target combinations for this analysis because these combinations have the smallest statistical and systematic errors. One can observe that within the statistical and systematic errors the results for the transverse momentum sum for fragments with $M=2$ are identical to the results for fragments with $M=1$. This observation can be interpreted as a breakup process for reactions with more than one heavy fragment produced in the interactions, which proceeds in more than one step: In the first step an excited projectile spectator is produced having almost the same transverse momentum as a projectile spectator, which does not break up into smaller fragments. In the second step the excited projectile spectator disintegrates into several fragments. This process gives an additional contribution to the transverse momenta of the finally detectable fragments. This second contribution consists probably of a contribution due to the mutual Coulomb repulsion between the produced fragments and an additional contribution due to the statistical breakup procedure itself. (This contribution could be described possibly by the Goldhaber model.)

VI. CONCLUSION

In this paper we have analyzed target and projectile energy dependences of transverse momentum distributions of fragments produced in reactions of ^{208}Pb and ^{197}Au projectiles with targets ranging from CH_2 to Pb at projectile energies of 1.0, 10.6, and 158 GeV/nucleon. This study was performed separately for different fragmentation processes. We distinguish between spallation, fission, and multifragmentation processes with one, two, or three detected fragments produced in the same interaction.

The investigation of the spallation reactions shows a significant projectile energy and target size dependence of the transverse momenta. Spallation reactions with the CH_2 target can be well described by the statistical model of Goldhaber at all projectile energies. For spallation reactions with the heavier targets, the measured transverse momentum distributions show contributions by different processes. Beside the statistical contribution, described by the model of Goldhaber, an additional contribution caused by the Coulomb repulsion between the projectile and target nucleus is observed. The dependence on the projectile energy, especially for the reactions with the Pb target, can be qualitatively explained by an additional contribution to projectile fragmentation by the process of electromagnetic dissociation. This dominates for reactions of ^{208}Pb projectiles with a Pb target at 158 GeV/nucleon. Since electromagnetic dissociation can happen for nuclear interactions at distances larger than the sum of the nuclear radii, the contribution by the Coulomb repulsion is reduced under these conditions.

The analyzed fission processes show, however, no significant projectile energy and target size dependences. The observed comparatively large values for the transverse momenta can be explained by the mutual Coulomb repulsion between the two produced heavy fragments of almost similar size.

The investigation of the multifragmentation reactions is more complicated. We have distinguished between multifragmentation reactions with one, two, or three detected fragments produced in the interactions. We found no differences between the results for the transverse momentum distributions for events with two or three detected fragments. But multifragmentation events with one detected fragment differ at least at 10.6 and 158 GeV/nucleon significantly from the results with more than one detected fragment. Furthermore, for these fragments, a significant projectile energy dependence can be observed. For multifragmentation events with two or three detected fragments only a weak projectile energy dependence can be found. Significant target size dependences for fragments produced in multifragmentation reactions can only be observed for the heavier fragments.

The comparison of the results for the distributions of transverse momenta for events with $M=1$ and the results for the transverse momentum sum of fragments with $M=2$ reveals that the breakup process for multifragmentation reac-

tions can be described if one assumes a breakup that proceeds in more than one step: In the first step an excited projectile spectator is generated disintegrating somewhat later into smaller fragments for which the mutual Coulomb repulsion contributes significantly to the measured transverse momentum.

ACKNOWLEDGMENT

We thank the staff of the GSI/SIS, BNL/AGS, and CERN/SPS for the excellent support during the exposures. This work was funded by the BMBF under Contract No. 06Si3673.

[1] A. Goldhaber, Phys. Lett. B **53**, 306 (1974).
[2] D. Greiner, P. Lindstrom, H. Heckman, B. Cork, and F. Bieser, Phys. Rev. Lett. **35**, 152 (1975).
[3] Y. Viyogi, T. Symons, P. Doll, D. Greiner, H. Heckman, D. Hendrie, P. Lindstrom, J. Mahoney, D. Scott, K. van Bibber, G. Westfall, H. Wieman, H. Crawford, C. McParland, and C. Gelbke, Phys. Rev. Lett. **42**, 33 (1979).
[4] F. Brady, W. Christie, J. Romero, C. Tull, B. McEachern, M. Webb, J. Young, H. Crawford, D. Greiner, P. Lindstrom, and H. Sann, Phys. Rev. Lett. **60**, 1699 (1988).
[5] J. Dreute, W. Heinrich, G. Rusch, and B. Wiegel, Phys. Rev. C **44**, 1057 (1991).
[6] F. Brady, W. Christie, J. Romero, C. Tull, J. Chance, P. Grim, J. Young, H. Crawford, T. Kobayashi, P. Lindstrom, D. Olson, T. Symons, I. Tanihata, H. Wieman, W. Müller, H. Sann, and U. Lynen, Phys. Rev. C **50**, R525 (1994).
[7] G. Rusch, W. Heinrich, B. Wiegel, E. Winkel, and J. Dreute, Phys. Rev. C **49**, 901 (1994).
[8] H. Custafsson, H. Gutbrod, B. Kolb, H. Löhner, B. Ludewigt, A. Poskanzer, T. Renner, H. Riedesel, H. Ritter, A. Warwick, F. Weik, and H. Wiemann, Phys. Rev. Lett. **52**, 1590 (1984).
[9] S. Wang, S. Barwick, D. Ifft, P. Price, and A. Westphal, Nucl. Instrum. Methods Phys. Res. B **35**, 43 (1988).
[10] G. Hüntrup, T. Streibel, and W. Heinrich, Phys. Rev. C **61**, 034903 (2000).
[11] V. Lindenstruth, Ph.D. thesis, Universität Frankfurt, 1993.
[12] K. Sümmerer, W. Brüchle, D. Morissey, M. Schädel, B. Szwezyn, and Y. Weifan, Phys. Rev. C **42**, 2546 (1990).
[13] H. Jaqaman and D. Gross, Nucl. Phys. **A524**, 321 (1991).
[14] E. Moniz, I. Sick, R. Whitney, J. Ficenec, R. Kephart, and W. Trower, Phys. Rev. Lett. **26**, 445 (1971).